Structure and energetics of mixed ^{4}He-^{3}He drops

M. Barranco and M. Pi
Departament d'Estructura i Constituents de la Matèria, Facultat de Física, Universitat de Barcelona, E-08028 Barcelona, Spain

S. M. Gatica and E. S. Hernández
Departamento de Física, Facultad de Ciencias Exactas y Naturales, Universidad de Buenos Aires, 1428 Buenos Aires, Argentina

J. Navarro
IFIC (Centro Mixto CSIC Universitat de València), Facultat de Física, E-46100 Burjassot, València, Spain
(Received 8 April 1997)

Using a finite-range density functional, we have investigated the energetics and structural features of mixed helium clusters. The possibility of doping the cluster with a molecule of sulfur hexafluoride is also considered. It is seen that the repulsion introduced by the impurity strongly modifies the properties of the smallest drops. Although only a qualitative comparison is possible, the gross features displayed by our calculations are in agreement with recent experimental findings. [S0163-1829(97)02438-7]

I. INTRODUCTION

Despite its considerable difficulty, the study of liquid helium drops has been a subject of great theoretical and experimental interest.[1,2] Up to very recently, the major limitations have been the experimental impossibility of selecting and identifying clusters of a given size, or at least, within a narrow size distribution, and the fact that most experiments were carried out on $^4\mathrm{He}_N$ clusters. These issues prevented a sensible comparison with available calculations and rendered academic some of the published theoretical studies, discouraging further investigations within the reach of theorists.

The situation is rapidly improving. Better scattering deflection methods are now able to size-select large helium clusters,[3] and molecular beam diffraction from a transmission grating seems able to do the same for small van der Waals clusters.[4] The drops can then be analyzed and the data compared with theory, a possibility that not long ago was unthinkable.

A field of emerging interest nowadays, is the analysis of pure and mixed ^{3}He-^{4}He clusters with doping atoms or molecules. The best studied systems are ^{4}He clusters doped with atomic impurities and SF_6 molecules (see Refs. 5–11, and references therein). The major outcomes of that body of work are to have established the location of the impurity in the bulk of the drop, and the fact that due to their low temperature, which is around 0.4 K for ^{4}He,[6] liquid drops provide useful ultracold matrices well suited for high resolution molecular spectroscopy. That temperature is even lower in the case of ^{3}He, some 0.15 K,[12] in good agreement with the predictions of Ref. 13.

Concerning pure ^{3}He drops, the first systematic study of their ground state properties was carried out by Pandharipande and co-workers using a variational Monte Carlo (VMC) technique,[14] and by Stringari and Treiner within a local, zero-range energy-density-functional (LDF) approximation.[15] There are also two recent systematic calculations which make use of nonlocal, finite-range density functionals (FRDF) built so as to reproduce a large number of properties of the homogeneous and inhomogeneous liquid.[16,17] Within LDF, a random-phase approximation calculation of the collective spectrum of close shell ^{3}He drops is also available.[18] FRDF results for open-shell ^{3}He droplets has also been reported.[19] As we have indicated, the theoretical effort have been hampered so far by the lack of experimental results on ^{3}He drops on one hand, and of a full microscopic theory, in contradistinction with the ^{4}He case, on the other hand.

In this work we present an investigation of $^3\mathrm{He}_N-^4\mathrm{He}_M$ and $^3\mathrm{He}_N-^4\mathrm{He}_M+\mathrm{SF}_6$ drops, systems for which experimental results are becoming available.[12] Previous calculations were carried out for one ^{3}He impurity in ^{4}He drops.[20,21] In particular, in Ref. 20 a zero-range density functional was employed to describe both the ^{4}He drop and the ^{3}He-^{4}He interaction. However, it has been recognized that functionals of this kind are not accurate enough to deal with finite-size effects, especially when the drop hosts an impurity that provokes a strong density compression. These drawbacks are removed by the inclusion of finite range interaction terms in the density functional; for this sake, in the present approach we introduce a FRDF adequate to describe properties of helium mixtures, which is presented in Sec. II, together with the method of calculation. The results for ^{4}He drops doped with one ^{3}He atom are presented in Sec. III, and IV for mixed drops. Finally, we draw our conclusions in Sec. V.

II. THE FINITE-RANGE DENSITY FUNCTIONAL FOR MIXED HELIUM DROPS

We consider that the total energy of a liquid-helium mixture can be expressed as a density functional of their particle densities ρ_3,ρ_4, and of the kinetic energy density τ_3 of ^{3}He:

$$E[\rho_3,\tau_3,\rho_4]=\int d\vec{r}\{\mathcal{E}_4[\rho_3,\rho_4]+\mathcal{E}_3[\rho_3,\tau_3,\rho_4]+\mathcal{E}_{34}[\rho_3,\rho_4]\},\quad(1)$$

where

TABLE I. Parameters of the density functional.

b_4 (K Å^3)	c_4' (K Å^6)	c_4'' (K Å^9)	b_3 (K Å^3)	$c_3'+c_3''$ (K Å$^{3+\gamma_3}$)	c_3'' (K Å$^{3+\gamma_3}$)	γ_3
-718.99	-2.41186×10^4	1.85850×10^6	-684.676	1.55379×10^6	-3.5×10^4	2.1251
b_{34} (K Å^3)	c_{34} (K Å$^{3+\gamma_{34}}$)	γ_{34}	α_s (K^{-1}Å^3)	ρ_{0s} (Å^{-3})	ρ_{3c} (Å^{-3})	ρ_{4c} (Å^{-3})
-662.8	4.5×10^6	2.6565	54.31	0.04	0.0406	0.062
ϵ_{LJ} (K)	h_3 (Å)	h_4 (Å)	h_{34} (Å)	σ_3 (Å)	σ_4 (Å)	σ_{34} (Å)
10.22	2.11311	2.190323	2.176374	2.46	2.556	2.5455

$$\mathcal{E}_4[\rho_3,\rho_4]=\frac{\hbar^2}{2m_4}(\nabla\sqrt{\rho_4(\vec{r})})^2+\frac{1}{2}\int d\vec{r}'\rho_4(\vec{r})V_4(|\vec{r}-\vec{r}'|)\times\rho_4(\vec{r}')+\frac{1}{2}c_4'\rho_4(\vec{r})[\overline{\rho_3}(\vec{r})+\overline{\rho_4}(\vec{r})]^2+\frac{1}{3}c_4''\rho_4(\vec{r})[\overline{\rho_3}(\vec{r})+\overline{\rho_4}(\vec{r})]^3-\frac{\hbar^2}{4m_4}\alpha_s\int d\vec{r}'F(|\vec{r}-\vec{r}'|)\left[1-\frac{\widetilde{\rho}_4(\vec{r})}{\rho_{0s}}\right]\times\nabla\rho_4(\vec{r})\cdot\nabla\rho_4(\vec{r}')\left[1-\frac{\widetilde{\rho}_4(\vec{r}')}{\rho_{0s}}\right], \tag{2}$$

$$\mathcal{E}_3[\rho_3,\tau_3,\rho_4]=\frac{\hbar^2}{2m_3^*}\tau_3+\frac{1}{2}\int d\vec{r}'\rho_3(\vec{r})V_3(|\vec{r}-\vec{r}'|)\rho_3(\vec{r}')+\frac{1}{2}c_3'\rho_3^2(\vec{r})[\overline{\rho_3}(\vec{r})+\overline{\rho_4}(\vec{r})]^{\gamma_3}+\frac{1}{2}c_3''\rho_3^2(\vec{r})\overline{\rho_3}(\vec{r})^{\gamma_3}, \tag{3}$$

$$\mathcal{E}_{34}[\rho_3,\rho_4]\}=\int d\vec{r}'\rho_3(\vec{r})V_{34}(|\vec{r}-\vec{r}'|)\rho_4(\vec{r}')+c_{34}\rho_3(\vec{r})\rho_4(\vec{r})[\overline{\rho_3}(\vec{r})+\overline{\rho_4}(\vec{r})]^{\gamma_{34}}. \tag{4}$$

In these expressions, $\overline{\rho_i}(\vec{r})$ for $i=3,4$ is an averaged density given by

$$\overline{\rho_i}(\vec{r})=\int d\vec{r}'\rho_i(\vec{r}')w_i(|\vec{r}-\vec{r}'|), \tag{5}$$

where

$$w_i(|\vec{r}|)=\frac{3}{4\pi h_i^3}\ \text{if}\ |\vec{r}|<h_i,\qquad 0\quad\text{otherwise}. \tag{6}$$

In addition, $V_i(|\vec{r}-\vec{r}'|)$ ($i=3$, 4 or 34) is a finite range interaction consisting of a Lennard-Jones (LJ) potential with truncated core

$$V_i(r)=4\epsilon_{LJ}\left[\left(\frac{\sigma_i}{r}\right)^{12}-\left(\frac{\sigma_i}{r}\right)^{6}\right]\quad\text{if}\ r\geqslant h_i,\qquad 0\quad\text{otherwise} \tag{7}$$

and $F(|\vec{r}-\vec{r}'|)$ is a Gaussian kernel with dispersion l equal to unity:

$$F(r)=\frac{1}{\pi^{3/2}l^3}e^{-r^2/l^2}, \tag{8}$$

which is also used to define the other averaged density entering $\mathcal{E}_4$:

$$\widetilde{\rho}_4(\vec{r})=\int d\vec{r}'\rho_4(\vec{r}')F(|\vec{r}-\vec{r}'|). \tag{9}$$

$\mathcal{E}_4$ reduces to the Orsay-Trento (OT) density functional[22] setting ρ_3 to zero. $\mathcal{E}_3$ and $\mathcal{E}_{34}$ are finite-range generalizations of the density functional introduced in Ref. 23 (see also Ref. 24), from where we have also taken the parametrization of the effective mass of ^{3}He, which was selected so as to fit the experimental data presented in Ref. 25:

$$\frac{\hbar^2}{2m_3^*}=\frac{\hbar^2}{2m_3}\left(1-\frac{\overline{\rho_3}}{\rho_{3c}}-\frac{\overline{\rho_4}}{\rho_{4c}}\right)^2. \tag{10}$$

The use of the OT functional makes it necessary to readjust the value of some of the original parameters entering $\mathcal{E}_3$ and $\mathcal{E}_{34}$. We have also changed σ_3 from its standard value to exactly reproduce the experimental surface tension of liquid ^{3}He that otherwise would have been some 10% higher. The size of the vanishing LJ cores h_i in Eq. (7) has been fixed as indicated in Ref. 24 and the remaining parameters so as to get the best possible fit to the maximum solubility x_M of ^{3}He into liquid ^{4}He, the excess volume coefficient and the osmotic pressure at various pressures between 0 and 20 atm for the liquid helium mixtures, together with the surface tension of the ^{3}He-^{4}He interface at zero temperature and saturation pressure. The set of coefficients of the whole density func-

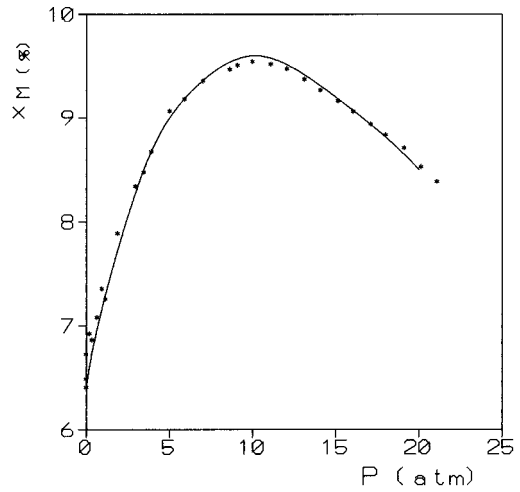

FIG. 1. The maximum solubility of ^{3}He into liquid ^{4}He in % as a function of pressure in atm. The experimental points have been taken from Ref. 32.

tional (1) is given in Table I. In this table, the quantity b_i is the volume integral of the corresponding LJ potential[22]

$$b_i = \int d\vec{r} V_i(|\vec{r}|). \tag{11}$$

Altogether, we have achieved an accurate description of the above mentioned thermodynamical properties of the mixture and its interfaces. For the sake of an example, we show in Fig. 1 the maximum solubility, and in Fig. 2 the surface tension of the ^{3}He-^{4}He interface as a function of pressure. These two magnitudes were only roughly described previously.[23]

For a cluster made of given number of atoms of each type N_4 and N_3, their structure and energetics result from the solution of the coupled Hartree[26] and Hartree-Fock[27] equations corresponding to each isotope, easily deduced from Eq. (1).[22,27] In the case of ^{3}He, the particle and kinetic energy densities are obtained from the single particle wave functions $\phi_j(\vec{r})$

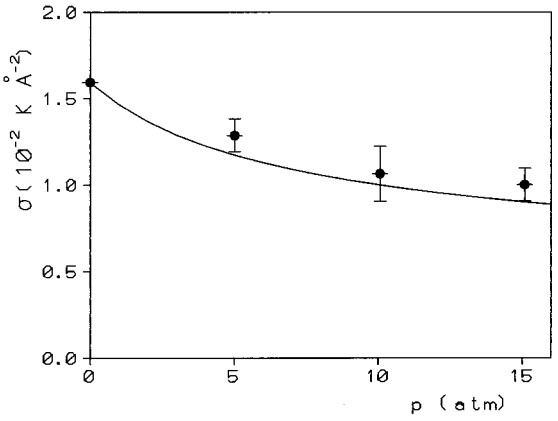

FIG. 2. The surface tension of the ^{3}He-^{4}He interface as a function of pressure in atm together with experimental data from Ref. 33.

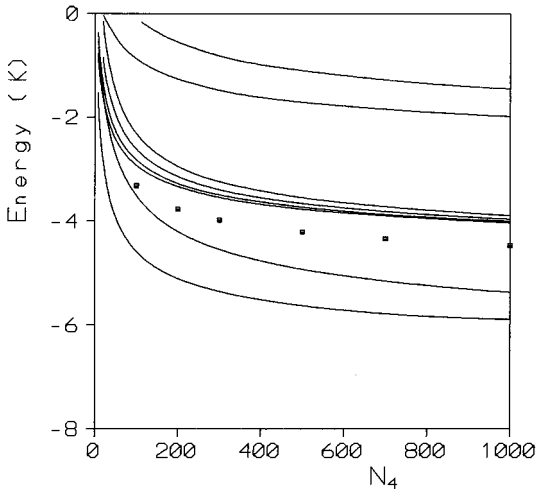

FIG. 3. From bottom to top the curves respectively represent, in K, the chemical potential μ_4, the energy per particle E_4/N_4, the single particle energies of states $1s$, $1p$, $1d$, $1f$, $2s$, and $3s$ of one ^{3}He atom, as functions of N in $^4\mathrm{He}_N$ clusters. The squares correspond to the $1s$ energies reported in Ref. 20.

$$\rho_3(\vec{r}) = \sum_{j=1}^{N_3} |\phi_j(\vec{r})|^2 = \sum_{nlm} \left| \frac{R_{nl}(r)}{r} Y_{lm}(\hat{r}) \right|^2, \tag{12}$$

$$\tau_3(\vec{r}) = \sum_{j=1}^{N_3} |\nabla \phi_j(\vec{r})|^2. \tag{13}$$

The diagonal part of the center-of-mass correction[27] has been taken into account making the following substitutions in the kinetic energy terms:

$$\frac{\hbar^2}{2m_3} \to \frac{\hbar^2}{2m_3}\left(1 - \frac{1}{N_3 + (m_4/m_3)N_4}\right), \tag{14}$$

$$\frac{\hbar^2}{2m_4} \to \frac{\hbar^2}{2m_4}\left(1 - \frac{1}{N_4 + (m_3/m_4)N_3}\right). \tag{15}$$

As in previous investigations concerning ^{4}He drops,[7,8,20] when we consider the possibility of the cluster being doped with sulfur hexafluoride, the molecule is regarded as an object with infinite mass located at the coordinate origin and providing an external field to all helium atoms. The potential for the spherically averaged SF_6-He potential, which should be added to either single particle (SP) mean field, is taken from Ref. 28.

III. SYSTEMATICS OF A SINGLE ^{3}He ATOM IN PURE AND DOPED ^{4}He DROPLETS

As we add one single ^{3}He atom to a given ^{4}He cluster, a variety of energetic features can be investigated as a function of the number of particles in the droplet N_4. After self-consistently determining the energy per particle E_4/N_4 and the chemical potential μ_4 of the ^{4}He atoms, the peculiarities of the ^{3}He spectrum depend upon N_4 as visualized in Figs. 3–6.

In Fig. 3 we display the single particle energies of the four lowest lying levels of this spectrum, as well as those of the

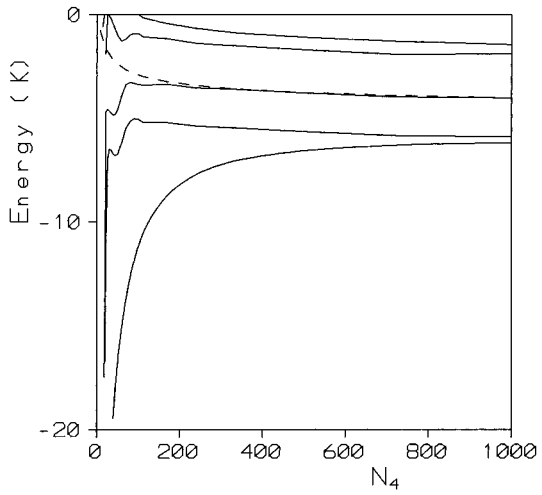

FIG. 4. From bottom to top the curves respectively represent, in K, the chemical potential μ_4, the energy per particle E_4/N_4, the SP energies of states $1s$, $2s$ and $3s$ of one ^{3}He atom, as functions of the N in doped $^4\mathrm{He}_N+\mathrm{SF}_6$ clusters. The dashed line corresponds to the $1s$ energy of the ^{3}He atom in the pure droplets.

next two higher s states, as functions of N_4. The squares indicate the $1s$ energies presented in Ref. 20. For completeness, we plot as well the energy per particle and chemical potential of the host cluster. We can realize that the present FRDF is more repulsive on ^{3}He atoms than the zero-range one employed in Ref. 20; this feature also shows up when we fit the trend of ε_{1s} to a mass formula of the type

$$\varepsilon_{1s}=\varepsilon_0+\frac{C}{N_4^{1/3}}, \tag{16}$$

with $\varepsilon_0 = -4.81$ K and $C=8.44$ K.[29] These parameters have been obtained including drops as large as $N_4 = 10^4$. Representing ε_0 the chemical potential of the ^{3}He atom on the surface of liquid ^{4}He at zero pressure, we observe that the

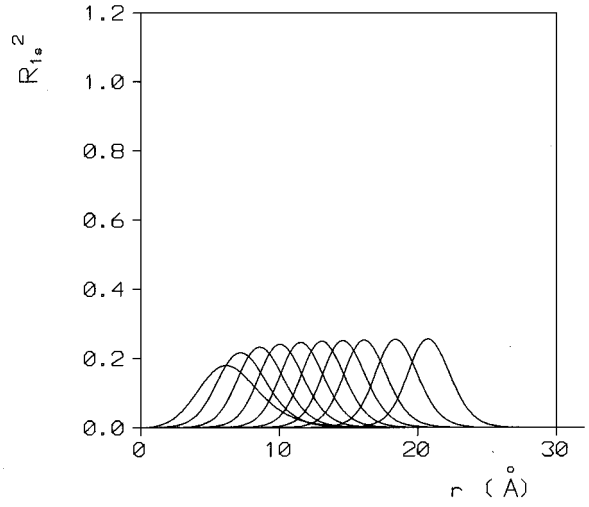

FIG. 5. The radial probability density $|R_{1s}(r)|^2$ of the ^{3}He atom in $^4\mathrm{He}_N$ as a function of the distance to the center of the droplet for, from left to right, $N_4=8$, 20, 40, 70, 112, 168, 240, 330, 500, and 728.

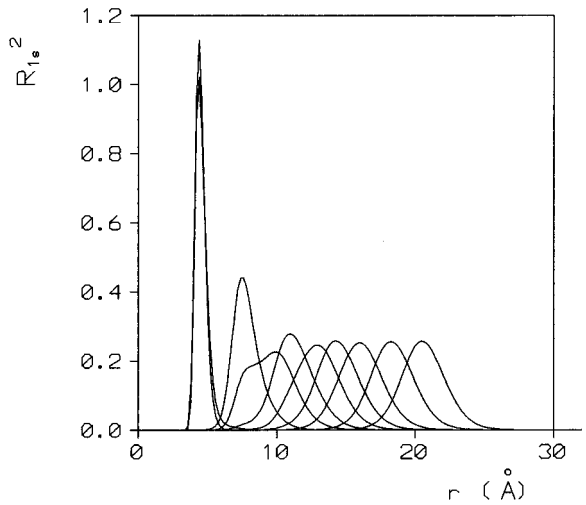

FIG. 6. Same as Fig. 5 for $^4\mathrm{He}_N+\mathrm{SF}_6$.

current value is reasonably close to the energy of the Andreev state, namely, $\varepsilon_0=(-5.00\pm0.03)$ K.[30] Notice that in Ref. 20, the corresponding values are $\varepsilon_0=-5.44$ K and $C=9.8$ K, and that the variational Monte Carlo calculation of[21] yields $\varepsilon_0\sim-4.90$ K. It is also apparent from this figure that as the size of the ^{4}He cluster increases, the spectrum of the ^{3}He atom becomes rather independent of the orbital quantum number. The rate of degeneracy is higher for states with radial quantum number equal to unity; this tendency can be confirmed examining the corresponding wave functions and their mean square radius, which become almost coincident when the drop contains a few hundreds of particles. This degeneracy reflects the physical fact that in the limit of a large drop, the surface ^{3}He states would no longer be adequately characterized by an angular momentum quantum number, but rather by a linear momentum parallel to the free surface, whose multipolar decomposition will in practice need a large superposition of partial waves.

An interesting property, already observed by Dalfovo,[20] is that as the number of nodes of the ^{3}He radial wave functions increases, the corresponding probability densities $|R_{nl}(r)|^2$ drift towards smaller rms radii; in particular, we find that while $|R_{1s}(r)|^2$ remains centered at distances slightly larger than the rms radius of the cluster, at least for the values of N_4 here considered, the $3s$ wave functions penetrate the drop if N_4 is above 200.

Figure 4 is similar to the former for ^{4}He drops doped with SF_6, but only the energies of s states are shown, since the energies of the lowest lying l levels rapidly become degenerate as the ^{4}He drop grows above a few tens of particles. In this case we appreciate that the distortion of the SP potential provided by the external field associated to the molecular impurity is important for the smallest drops, namely, for N_4 below 300. This behavior was observed in Ref. 31 in connection with the systematics of pure and doped ^{4}He clusters; for the sake of additional comparison, the 1s energy of the ^{3}He atom in the pure droplets is displayed in dashed lines, showing that ε_{1s} is insensitive to the presence of the SF_6 molecule for these large values of N_4. In this case, we observe that in the same range of drop sizes, the molecular field strongly binds the ^{3}He atom and at the same time, it lowers

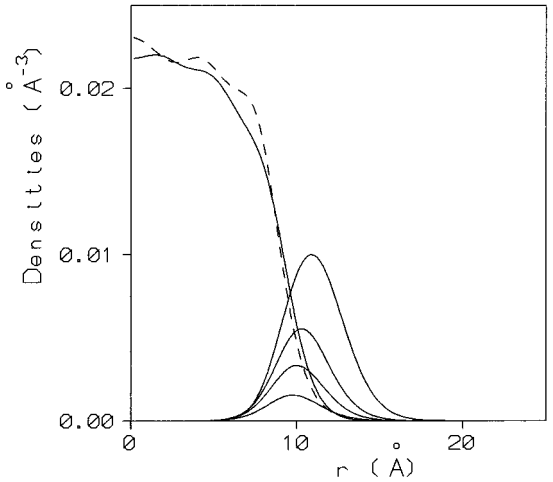

FIG. 7. The densities $\rho_4(r)$ (Å^{-3}) of the $^4He_{70}$ drop for $N_3=8$ (full line) and 72 (dashed line), and $\rho_3(r)$ (Å^{-3}) for $N_3=8$, 18, 32, and 72 from bottom to top, as functions of r (Å).

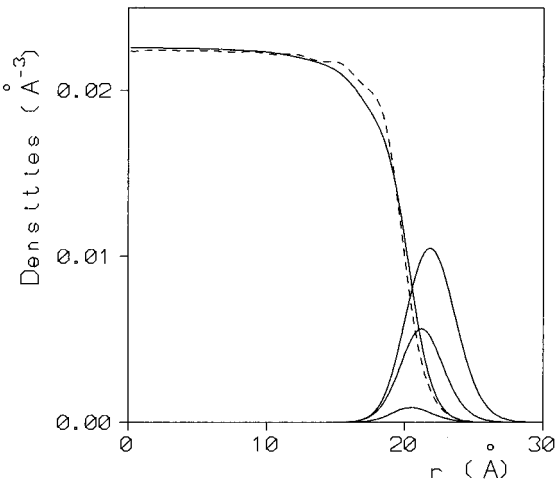

FIG. 9. The densities $\rho_4(r)$ (Å^{-3}) of the $^4He_{728}$ drop for $N_3=18$ (full line) and 288 (dashed line), and $\rho_3(r)$ (Å^{-3}) for $N_3=18$, 128, and 288 from bottom to top, as functions of r (Å).

and compresses the whole spectrum to a significant amount. The effect of the SF_6 potential on the ^{3}He systematics disappears for N_4 above 300, due to the fact that at the distances where the wave functions $\phi_j(\vec{r})$ concentrate, the molecular potential is almost vanishing. The source for the ^{3}He potential is the density $\rho_4(\vec{r})$, which at these radii is also rather insensitive to the presence of the impurity.

In Fig. 5 we show the radial probability density $|R_{1s}(r)|^2$, as a function of the distance to the center of the droplet for different N_4. Figure 6 displays the same quantity for the corresponding doped drops. A comparison of these two pictures indicates that for the smaller drop sizes the foreign molecule not only prevents the ^{3}He atom from reaching the central region, but compresses the whole pattern. For every N_4, the ^{3}He atom is pushed towards smaller radii; we can also observe that for the $^4He_{70}$ drop, two peaks have developed and the outer one becomes the most important as the drop size keeps growing. For $N_4=112$ the peak lies slightly to the left of the corresponding one in the pure cluster, whose height it moderately exceeds, remaining more concentrated. For N_4 larger than 300, the probability densities are very similar, indicating that the presence of the molecular impurity has little influence on the ^{3}He surface states (Andreev states). It is worthwhile noticing that the accuracy of this type of calculations has been recently found comparable[31] to that of variational descriptions of small clusters of liquid ^{4}He.[9]

IV. THE CASE OF PURE AND DOPED ^{4}He DROPLETS WITH VARIABLE NUMBER OF ^{3}He ATOMS

As a case of study, in this section we shall concentrate our analysis on two ^{4}He clusters of rather different size, namely, $N_4=70$ and 728. In Fig. 7 we show the densities $\rho_4(r)$ and $\rho_3(r)$ for different N_3 values between 8 and 72, as functions of the radial distance, for the $^4He_{70}$ drop. The number of

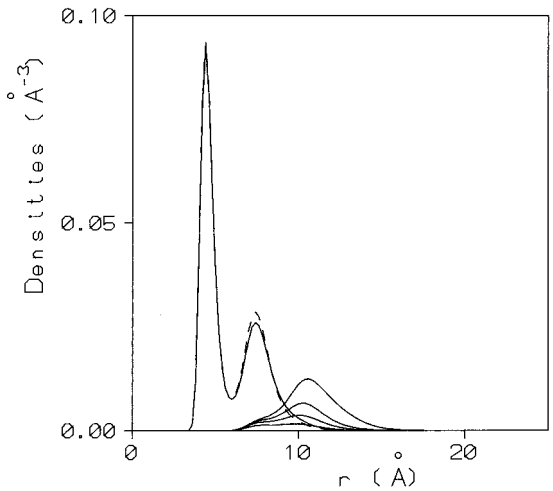

FIG. 8. The densities $\rho_4(r)$ (Å^{-3}) of the $^4He_{70}$ + SF_6 drop for $N_3=8$ (full line) and 72 (dashed line), and $\rho_3(r)$ (Å^{-3}) for $N_3=8$, 18, 32, and 72 from bottom to top, as functions of r (Å).

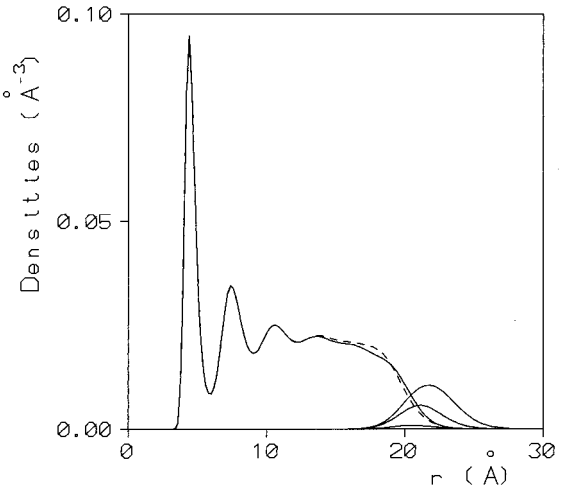

FIG. 10. The densities $\rho_4(r)$ (Å^{-3}) of the $^4He_{728}$ + SF_6 drop for $N_3=18$ (full line) and 288 (dashed line), and $\rho_3(r)$ (Å^{-3}) for $N_3=18$, 128, and 288, from bottom to top, as functions of r (Å).

TABLE II. Energetics of mixed drops. $N_4=70$ pure (columns 2–4) and doped with SF_6 (columns 5–7).

N_3	$E/(N_3+N_4)$ (K)	μ_4 (K)	μ_3 (K)	$E/(N_3+N_4)$ (K)	μ_4 (K)	μ_3 (K)
0	−2.97	−4.17		−12.95	−5.46	
8	−3.06	−4.35	−2.68	−12.72	−5.38	−3.28
18	−3.00	−4.45	−2.59	−11.62	−5.39	−3.13
32	−2.92	−4.60	−2.47	−10.42	−5.49	−2.96
50	−2.81	−4.80	−2.29	−9.25	−5.63	−2.68
72	−2.68	−5.05	−2.08	−8.16	−5.80	−2.31

^{3}He atoms has been chosen so as to fill a shell of their single-particle spectrum. Figure 8 shows the same magnitudes for the cluster $^4He_{70}$ + SF_6. We may notice in these two pictures a slight tendency of $\rho_3(r)$ to penetrate more deeply into the pure host cluster. It should be remarked that whatever the value of N_3, the density ρ_3 remains peaked at the surface of the $^4He_{70}$ drop; we can observe as well a slight inward compression of this surface as the ^{3}He bubble grows larger. In Fig. 8, an inner peak in ρ_3 that insinuates for high N_3 may indicate the attraction of the low ^{4}He density in the dip of the drop profile, intending to build a new ''Andreev-like'' state. Up to the largest N_3 value we have considered for this cluster, namely, 72, we have not found any evidence of the ^{3}He atoms diluting in the bulk of the drop.

Figures 9 and 10 are the same as Figs. 7 and 8 for $N_4=728$. It is clear that in any configuration, the density $\rho_3(r)$ definitely sits at the surface of the drop even for the largest configuration we have studied. It is also clear that the larger the hosting ^{4}He drop, the larger its surface and consequently, the higher the number of ^{3}He atoms it may accommodate. The above mentioned compressional effect induced by the latter on the bosonic cluster is also present.

Concerning the energy systematics of these systems, the major characteristics we report are that increasing amounts of ^{3}He atoms introduce important attractive contributions into the chemical potential of the ^{4}He atoms, and repulsive ones in the chemical potential of ^{3}He atoms. Also, the drops become less bound as we increase N_3 at fixed N_4. This is due to the energy per particle difference between liquid ^{3}He and ^{4}He, −2.49 and −7.15 K, respectively. These facts can be visualized in Table II, where we show the total energy per particle and the chemical potentials of ^{4}He and ^{3}He for pure and doped $^4He_{70}$ clusters as functions of N_3. Table III contains the same quantities for $^4He_{728}$ drops. Observing these behaviors we realize that the presence of an impurity modifies the energetics to an important amount in the cluster $N_4=70$, providing stronger binding in all the cases here shown; this effect, however, becomes less significant for larger number of ^{4}He atoms.

V. SUMMARY

In this work we have performed a detailed study of the energetics and structure of mixed ^{3}He-^{4}He clusters, either pure or doped with a SF_6 molecule. For this sake, we have used a new density functional that improves previous descriptions of liquid helium mixtures and that through the explicit incorporation of finite-range interaction terms, provides a good adjustment of the surface tensions of the ^{3}He and ^{4}He free surfaces and of the ^{3}He-^{4}He liquid interface. We have considered, on the one hand, the type of spectrum and ground-state wave functions that a pure or a doped ^{4}He drop furnishes to one ^{3}He atom, and on the other, the density configurations of pure and doped clusters with various numbers of atoms of each class, N_3 and N_4.

In accordance with Refs. 20 and 21 the present investigation shows that a single ^{3}He atom immersed into a ^{4}He cluster has a SP spectrum whose lowest energy state smoothly approaches the Andreev state in the liquid-free surface; in this context, adding the molecular impurity modifies the structure and the energetics of these SP states only for the smallest numbers N_4. Increasing the number of ^{3}He atoms gives rise to interesting structural features, one of which is that ^{3}He atoms locate on the surface of the ^{4}He cluster regardless the particular combination (N_3, N_4), at least up to a few hundreds of atoms of either class. Taking into account that the structure of liquid mixtures, for concentrations above the maximum solubility of ^{3}He in ^{4}He, corresponds to an homogeneous ^{3}He-^{4}He solution plus a segregated phase consisting of pure ^{3}He, it is apparent from the present calculations that much larger amounts of atoms are needed to visualize the onset of ^{3}He dilution.

As a final remark, we would like to stress the fact that recently, large ^{3}He drops containing a small fraction of ^{4}He atoms and doped with sulfur hexafluoride have been produced and mass analyzed.[12] Experimental data and determination of the rotational constants for the SF_6 spectra indicate

TABLE III. Energetics of mixed drops. $N_4=728$ pure (columns 2–4) and doped with SF_6 (columns 5–7).

N_3	$E/(N_3+N_4)$ (K)	μ_4 (K)	μ_3 (K)	$E/(N_3+N_4)$ (K)	μ_4 (K)	μ_3 (K)
0	−5.16	−5.80		−6.30	−5.80	
18	−5.14	−5.80	−3.86	−6.24	−5.81	−3.87
128	−4.94	−5.89	−3.40	−5.90	−5.89	−3.40
288	−4.63	−6.08	−2.71	−5.44	−6.08	−2.70

that ^{4}He particles build up a first atom shell around the foreign molecule, in agreement with the present theoretical results.

ACKNOWLEDGMENTS

It is a pleasure to thank Professor J.P. Toennies and Dr. A. Vilesov for useful correspondence. This work has been performed under Grants Nos. EX071/95 from University of Buenos Aires, Argentina, PB95-1249 and PB92-0820 from CICYT, Spain, and Program GRQ94-1022 from Generalitat of Catalunya. One of us (E.S.H.) is grateful to the Department d'Estructura i Constituents de la Matèria (Universitat de Barcelona) for warm hospitality and support during various stays.

[1] J.P. Toennies, in *The Chemical Physics of Atomic and Molecular Clusters*, Proceedings of the International School of Physics ''Enrico Fermi,'' Course CVII, Varenna, 1988 (North-Holland, Amsterdam, 1990), p. 597.
[2] K.B. Whaley, Int. Rev. Phys. Chem. **13**, 41 (1994).
[3] M. Lewerenz, B. Schilling, and J.P. Toennies, Chem. Phys. Lett. **206**, 381 (1993).
[4] W. Schoellkopf and J.P. Toennies, Science **256**, 1345 (1994).
[5] S. Goyal, D. L. Schutt and G. Scoles, J. Phys. Chem. **97**, 2236 (1993).
[6] M. Hartmann, R. B. Miller, J. P. Toennies, and A. Vilesov, Phys. Rev. Lett. **75**, 1566 (1995).
[7] S. A. Chin and E. Krotscheck, Phys. Rev. B **52**, 10 405 (1995).
[8] E. S. Hernaández and M. Barranco, Phys. Rev. B **51**, 9364 (1995).
[9] M. A. McMahon, R. N. Barnett, and K. B. Whaley, J. Chem. Phys. **104**, 5080 (1996).
[10] F. Dalfovo, Z. Phys. D **29**, 61 (1994).
[11] G. De Toffol, F. Ancilotto, and F. Toigo, J. Low Temp. Phys. **102**, 381 (1996).
[12] J. Harms, M. Hartmann, J.P. Toennies, and A.F. Vilesov, J. Mol. Spectrosc. (to be published).
[13] A. Guirao, M. Pi and M. Barranco, Z. Phys. D **21**, 185 (1991).
[14] V.R. Pandharipande, S.C. Pieper, and R. B. Wiringa, Phys. Rev. B **34**, 4571 (1986).
[15] S. Stringari and J. Treiner, J. Chem. Phys. **87**, 5021 (1987).
[16] S. Weisgerber and P.-G. Reinhard, Z. Phys. D **23**, 275 (1992).
[17] M. Barranco, D. M. Jezek, E. S. Hernández, J. Navarro, and Ll. Serra, Z. Phys. D **28**, 257 (1993).
[18] Ll. Serra, J. Navarro, M. Barranco, and Nguyen Van Giai, Phys. Rev. Lett. **67**, 2311 (1991).
[19] M. Barranco, J. Navarro, and A. Poves, Phys. Rev. Lett. **78**, 4729 (1997).
[20] F. Dalfovo, Z. Phys. D **14**, 263 (1989).
[21] A. Belić, F. Dalfovo, S. Fantoni, and S. Stringari, Phys. Rev. B **49**, 15 253 (1994).
[22] F. Dalfovo, A. Lastri, L. Pricaupenko, S. Stringari, and J. Treiner, Phys. Rev. B **52**, 1193 (1995).
[23] F. Dalfovo, Ph.D. thesis, University of Trento, 1989.
[24] N. Pavloff and J. Treiner, J. Low Temp. Phys. **83**, 15 (1991).
[25] H. C. Chocolats, R. M. Mueller, J. R. Owers-Bradley, Ch. Buchal, M. Kubota, and F. Pobell, in *Low Temperature Physics LT17*, edited by U. Eckern, A. Schmid, W. Weber and H. Wuhl (Elsevier, New York, 1984).
[26] M. Casas, F. Dalfovo, A. Lastri, Ll Serra, and S. Stringari, Z. Phys. D **35**, 67 (1995).
[27] D. Vautherin and D. M. Brink, Phys. Rev. C **5**, 626 (1972).
[28] R. T. Pack, E. Piper, G. A. Pfeffer, and J. P. Toennies, J. Chem. Phys. **80**, 4940 (1984).
[29] Finite range density functionals yield density profiles having narrower surfaces than local density functionals. This is the reason why we find a better agreement with experiment than Ref. 20, see Ref. 21.
[30] D.O. Edwards and W.F. Saam, *Progress in Low Temperature Physics*, edited by D.F. Brewer (North Holland, Amsterdam, 1978), Vol. II A, p. 283.
[31] S. M. Gatica, E. S. Hernández, and M. Barranco, J. Chem. Phys. **107**, 927 (1997).
[32] C. Ebner and D. O. Edwards, Phys. Rep. **2**, 77 (1970).
[33] L.S. Balfour, Ph.D. thesis, Haifa, 1978.